Chemical Geology 356 (2013) 209–214

Contents lists available at ScienceDirect

Chemical Geology

journal homepage: www.elsevier.com/locate/chemgeo

# Magnesium isotope systematics of endoskarns: Implications for wallrock reaction in magma chambers

Bing Shen [a,b,*], Joshua Wimpenny [c], Cin-Ty A. Lee [b,**], Darren Tollstrup [c], Qing-Zhu Yin [c]

[a] School of Earth and Space Sciences, Peking University, Beijing 100871, PR China
[b] Department of Earth Science, Rice University, Houston, TX 77005, United States
[c] Department of Geology, University of California, Davis, CA 95616, United States

ARTICLE INFO

*Article history:*
Received 12 December 2012
Received in revised form 9 August 2013
Accepted 12 August 2013
Available online 17 August 2013

Editor: U. Brand

*Keywords:*
Endoskarn
Xenoliths
Mg isotope
Magma–wallrock reaction
Skarn

ABSTRACT

We measured the magnesium isotopic compositions of endoskarns (i.e., the metasomatically altered interior margin of the pluton) generated by contact metamorphism between granodioritic magma and dolomitic wallrock. The endoskarns were sampled as crustal xenoliths in Pleistocene basaltic cinder cones erupted in eastern California and provide a record of pluton–wallrock interactions at depth. The endoskarns consist of an outer zone made of pyroxenite (Mg-rich) and an inner zone represented by a plagioclase–quartz lithology with relict plutonic textures and minor pyroxene. The inner and outer zones are separated by a thin selvage of phlogopite. The Mg isotopic compositions of these endoskarns are all significantly lighter ($\delta^{26}Mg < -0.8‰$ relative to the Dead Sea magnesium (DSM-3) standard) than canonical peridotitic mantle ($\delta^{26}Mg = -0.25‰$). In particular, the outer pyroxenite zones of the endoskarn are consistently >1‰ lighter (−1.69 to −2.09‰; mean = −1.74‰; SD = 0.07‰; n = 8) than the mantle, and Mg isotopic values increase in the inner, Mg-poor and plagioclase–quartz dominated zone ($\delta^{26}Mg$ of −0.82‰). Because of the high temperatures associated with endoskarn formation, it is unlikely that the light Mg isotopic compositions result from equilibrium isotopic fractionations between mineral phases. The Mg isotopic signatures of the endoskarns are most easily interpreted by the mixing of Mg between Mg-rich and $^{26}Mg$-depleted dolomitic wallrock with Mg-poor and $^{26}Mg$-enriched magma. Mg isotopes may thus be useful in tracking magma–carbonate interactions in magmas.



## 1. Introduction

Crustal assimilation of wallrock or anatectic melts derived from the wallrock is an important process in the origin and differentiation of magmas. Of interest here is the assimilation of crustal carbonates, such as limestones and dolostones, which could lead to extensive decarbonation (Kerrick, 2001). Examples in which carbonate assimilation is thought to be a significant source of $CO_2$ in volcanoes come from Merapi in Indonesia (Chadwick et al., 2007) and Etna and Vesuvius in Italy (Allard et al., 1991; Fulignati et al., 2000). To place these types of volcanoes in context, Etna and Vesuvius ($1.3 \pm 0.3 \times 10^{13}$ g/yr $CO_2$) combined make up 20% of the modern day global $CO_2$ production from arcs ($<3.1 \times 10^{13}$ g/yr C) (Allard et al., 1991; Dasgupta and Hirschmann, 2010). If carbonate assimilation is widespread, then there are important implications for the long-term global carbon cycle and climate change (Kerrick, 2001; Berner, 2003; Lee et al., 2013).

The extent to which magmas interact with crustal carbonates, however, is difficult to constrain because the interaction zones are often poorly exposed. In many cases, crustal carbonates can be assimilated by magmas, leaving behind little physical evidence (Liao et al., 2012). Detecting carbonate assimilation in magmas using conventional radiogenic isotopes may be difficult because limestones and dolostones are typically characterized by unradiogenic Sr isotopes (and hence, similar to juvenile magmas), and their Nd concentrations are so low that they may not influence the Nd isotopic composition of the magma. Therefore, it is possible that the extent of carbonate assimilation in the evolution of magmas has been under-estimated. Diagnostic tools for identifying carbonate interaction/assimilation by magmas are thus necessary.

The stable isotopes of Mg may have potential in tracking carbonate wallrock and magma interactions. Significant Mg isotopic variations are observed in low temperature environments, ranging from +1‰ to ~−5.5‰ (Galy et al., 2002; Tipper et al., 2006a; Buhl et al., 2007; Brenot et al., 2008; Pogge von Strandmann et al., 2008; Tipper et al., 2008; Immenhauser et al., 2010; Li et al., 2010; Teng et al., 2010b; Wimpenny et al., 2010; Huang et al., 2012). For example, river waters vary from −2.6‰ to +0.8‰(Tipper et al., 2006a,b; Pogge von Strandmann et al., 2008; Tipper et al., 2008), weathering residues are between −0.3‰ and +0.6‰ (Teng et al., 2010b; Huang et al., 2012), seawater is globally homogeneous at ~−0.8‰ (Ling et al., 2011), and carbonates are between −1‰ to −5.5‰ (Galy et al., 2002; Pogge von Strandmann, 2008; Higgins and Schrag, 2010). In contrast, igneous

* Correspondence to: B. Shen, School of Earth and Space Sciences, Peking University, Beijing 100871, PR China.
** Corresponding author.
*E-mail address:* bingshen@pku.edu.cn (B. Shen).

0009-2541/$ – see front matter © 2013 Elsevier B.V. All rights reserved.
http://dx.doi.org/10.1016/j.chemgeo.2013.08.018

rocks and minerals generally exhibit a more limited range in Mg isotopic compositions (Handler et al., 2009; Liu et al., 2010; Teng et al., 2010a), although inter-mineral isotopic fractionations are also observed in high temperature rocks (Li et al., 2011; Liu et al., 2011; Wang et al., 2012).

Thus, given the sharp contrast in Mg isotopic behavior during low and high temperature processes, low temperature isotopic signals can be preserved during high temperature processes. As shown in recent studies by Shen et al. and Teng's group (Shen et al., 2009; Liu et al., 2010), some granitic rocks are isotopically heavy in Mg, which can be explained by the assimilation of pelitic metasediments, which are enriched in $^{26}$Mg (Li et al., 2010). However, assimilation of carbonate rocks, such as dolostones or Mg-bearing limestones, should drive Mg isotopes towards light signatures.

As a step towards testing the effect of carbonate assimilation on the Mg isotopes of magmas, we investigated rocks formed by the interaction of granodioritic magma with a dolomitic wall rock derived from the deep crust of the late Cretaceous Sierra Nevada batholith in California, USA (Ducea, 2001; Lee et al., 2007). These metasomatic interior margins of plutonic rocks are called endoskarns. These rocks were sampled as xenoliths hosted in Quaternary basaltic lavas associated with Basin and Range extension (Dyer et al., 2011). Previous detailed petrographic and geochemical analyses of these samples show that their protoliths are granodiorite plutonic rocks that have been metasomatized by $CO_2$-bearing fluids released from dolomitic wall rock due to decarbonation of the wall rock during skarn formation. Specifically, these $CO_2$-bearing fluids were also enriched in Ca and Mg, leading to Ca and Mg enrichment of the pluton margins, resulting in the formation of an endoskarn. In this paper, we investigate the Mg isotopic composition of endoskarns in order to assess the extent to which they inherit an isotopic signature from the carbonate wallrock. Because most endoskarn outcrops are poorly exposed or highly weathered, we examined Cretaceous endoskarn xenoliths in Pleistocene volcanoes. These endoskarns were sampled from depth during eruption, providing some of the freshest samples of endoskarn available.

## 2. Geological setting and sample description

The xenoliths analyzed in this study were collected from the Fish Springs alkali basalt cinder cone (N 37.0712, W 118.2550), which erupted ~0.314 million years ago (Martel et al., 1987; Blondes et al., 2008) on the eastern flank of the Sierra Nevada in the Big Pine volcanic field (0.1–0.5 m.y.) (Fig. 1) (Beard and Glazner, 1995; Mordick and Glazner, 2006; Blondes et al., 2008). The exposed basement rock through which the Big Pine volcanic field was emplaced is composed of Cretaceous granitoids to the west and Paleozoic metasediments to the east (Bateman, 1961; Kistler et al., 1965). Crustal xenoliths are abundant in the Fish Springs cinder cone. Petrographic and geochemical observations suggest that a subset of these crustal xenoliths is represented by endoskarns, formed by the interaction between granodioritic magmas and carbonate wallrocks (Dyer et al., 2011). The endoskarn xenoliths range in size from a few cm up to 30 cm. Notable features in these endoskarns include original igneous minerals that have been replaced by Ca-rich plagioclase and pyroxene (diopside), replacive pyroxenes preserving plagioclase trace-element signatures, and phlogopitic reaction zones between the pyroxene-rich skarn and magma (Dyer et al., 2011).

In this study, we focus on two xenolith samples. Sample A (Fig. 2) consists of four reaction zones with distinctive mineralogies. In the direction of wallrock to magma, these zones are: a pyroxenite zone (Px), a phlogopite-rich zone (Phl), a pyroxene-rich (~30%) plagioclase–quartz zone (Px–Q–Pl), and a plagioclase–quartz zone with <5% pyroxene (Pl–Q). This entire reaction zone occurs over a distance of ~10 cm and is typical of magma–wallrock contacts described in Dyer et al. The Px zone is considered the contact itself and all other zones are considered the endoskarn. Zone Pl–Q contains relict igneous textures and represents the outer margin of the pluton body (Dyer et al., 2011). The original plutonic mafic minerals (e.g., hornblende and biotite) are not present in zones Pl–Q and Px–Q–Pl, suggesting that they have been replaced by pyroxene. Sample B (Fig. 3) is a large (20 cm) plagioclase–quartz rock containing small amounts of pyroxene and occurring as finely

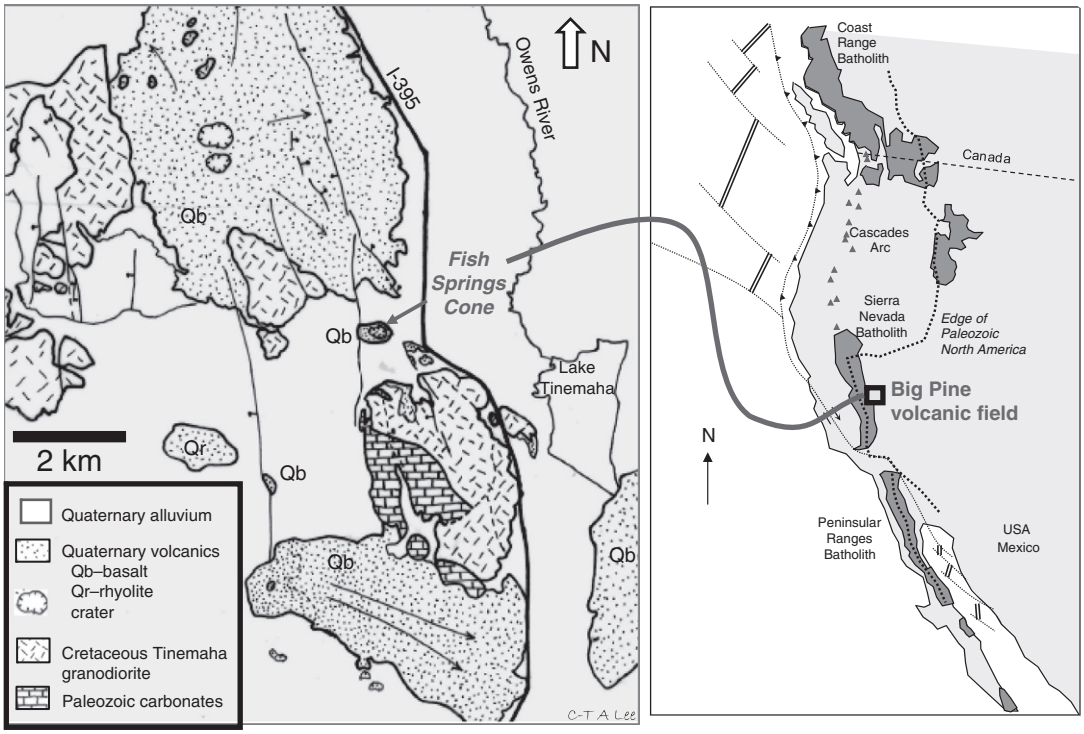


**Fig. 1.** Geological map showing the sample locality, the Fish Springs cone in the Big Pine volcanic field in the eastern edge of Sierra Nevada.

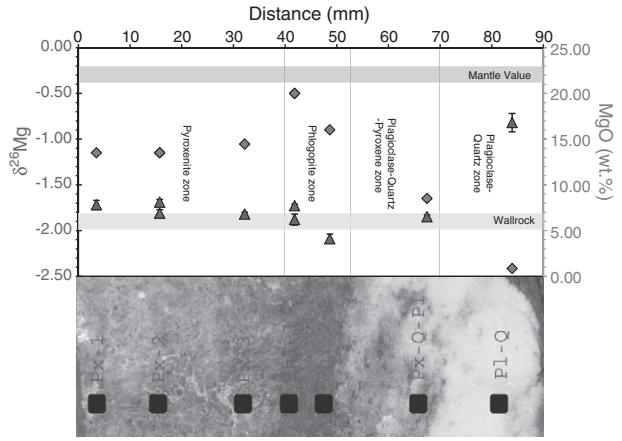


**Fig. 2.** Mg isotopic compositions (triangles and left-hand axis) and concentrations (diamonds and right-hand axis) are shown in the upper panel and photograph of Sample A with mineral zonation (lower panel). Error bars are 2 standard deviations; the red shadow area denotes the Mg isotopic composition of the mantle; the yellow shadow area represents the possible isotopic composition of dolomitic wallrock.

disseminated and sub-parallel bands in the rock. Although it contains no reaction zones, the lithology of Sample B closely resembles that of zone Px–Q–Pl in Sample A. These mineralogic zones also correspond to changes in whole-rock MgO content, which correlates with the mode of the Mg-bearing phase. All pyroxenes are of the diopside endmember and are characterized by 20–25 wt.% MgO (Dyer et al., 2011). Based on the above mineral modes, the reconstructed MgO contents of the Px zone are ~10–15 wt.%, the Px–Q–Pl zones are ~3–8 wt.% MgO, and the Pl–Q zone are <1 wt.% MgO. The Phl zone is characterized by ~15–20% MgO.

The above mineralogic zones result from reaction between the granodioritic magma and dolomite wallrock at depth. The pyroxenite zone (Px), composed almost of pure endmember diopside, formed by the following decarbonation reaction at the pluton–dolomite contact:

$$2Si^{4+} + 4H_2O + CaMg(CO_3)_2 \rightarrow CaMgSi_2O_6 + 8H^+ + 2CO_2\uparrow.$$

The phlogopite zone (Phl) occurs at the interface between the pyroxenite zone (Px) and the pyroxene-rich plagioclase–quartz zone (Px–Q–Pl). Phlogopite is the product of K-bearing magma reacting with the pyroxene zone:

$$2K^+ + 2Al^{3+} + 18H^+ + 6CaMgSi_2O_6 \rightarrow K_2Mg_6Si_6Al_2O_{20}(OH)_4 + 6Ca^{2+} + 6Si^{4+} + 12H_2O.$$

Pyroxenes in the Pl–Q and Px–Q–Pl zones represent replacement of magmatic plagioclase associated with Mg-rich fluids derived from the dolomite

$$Mg^{2+} + 4H^+ + CaAl_2Si_2O_8 \rightarrow CaMgSi_2O_6 + 2Al^{3+} + 2H_2O.$$

As discussed in Dyer et al., this reaction was evidenced by plagioclase–diopside replacement textures as well as pyroxenes with trace-element signatures inherited from plagioclase. The purpose of this study is to investigate how Mg isotopes vary across these reaction fronts.

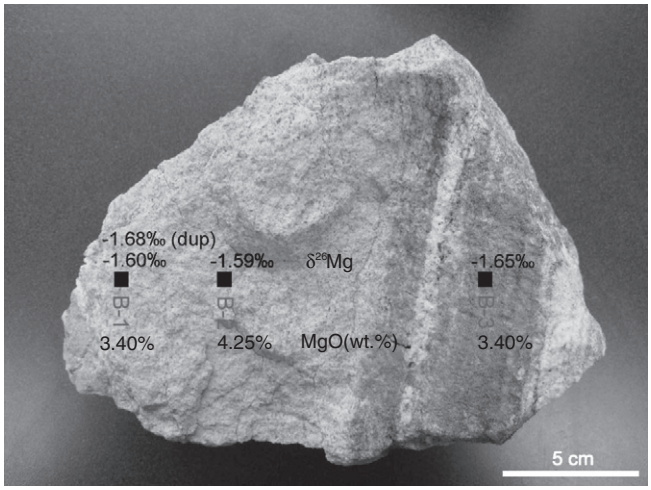


**Fig. 3.** Photograph of Sample B. Mg isotopic compositions ($\delta^{26}$Mg) and MgO (wt.%) are also marked on the photo.

## 3. Methods

### 3.1. Sample preparation

Three subsamples from the Px zone, two from the Phl zone, one from the Px–Q–Pl zone, and one from the Pl–Q zone were extracted from xenolith Sample A. Three subsamples were extracted from Sample B. Because the mafic minerals (pyroxene and phlogopite) account for all of the Mg in these lithologies, only mafic minerals were hand-picked from the coarse crushed sample (e.g., avoiding quartz and plagioclase) in order to decrease matrix effects and facilitate purification of Mg after dissolution. Between 4 and 40 mg of mafic mineral grains were dissolved in Savillex Teflon beakers using a mixture of concentrated HF and $HClO_4$. The samples were heated in sealed beakers overnight at 135 °C, then evaporated on a hot plate at 170 °C. This process was repeated before sample residues were dissolved in 2% $HNO_3$ in preparation for column chemistry.

### 3.2. Column chemistry

Mg was purified by cation exchange chromatography at Rice University. Two cation columns were used; column 1 was loaded with 1.8 ml of Bio-Rad AG50W-X12 resin (200–400 mesh) and used to separate Mg from Ca. Column 2, was loaded with 0.5 ml of Bio-Rad AG50W-X12 resin (200–400 mesh) and calibrated to separate Mg from all other matrices. Both columns are pre-cleaned by 6 N HCl, and conditioned with 12 N HCl and 1 N HCl, respectively.

Sample solutions containing ~15–20 μg of Mg were eluted through column 1 in 12 N HCl. Mg is collected in 4 ml of 12 N HCl with Ca being retained on the resin. The collected Mg-bearing solution was dried then loaded onto column 2 in 1 N HCl. This second column step involves the sequential elution of 0.8 ml of 1 N HCl, 4 ml of 1 N $HNO_3$ + 0.5 N HF, 1 ml of 1 N $HNO_3$, and 0.5 ml of 2 N $HNO_3$ to elute Cr, Al, Fe, Na, V, and K, respectively. Mg is then collected with 3 ml of 2 N $HNO_3$. To ensure a clean Mg fraction, each sample was passed through column 1 twice, followed by three to five passes through column 2. Final Mg fractions were analyzed by a single-collector inductively coupled plasma mass spectrometer (ICP-MS) at Rice University to assess the purity of the Mg. The Na/Mg, Al/Mg, K/Mg, Ca/Mg, and Fe/Mg are all less than 5% in the final solution, and the Mg recovery is >99%.

### 3.3. Mass spectrometry

Mg isotope ratios were measured at the University of California, Davis using a Thermo Scientific *Neptune Plus* high-resolution multiple-collector ICP-MS. Solutions containing 500 ppb Mg were introduced into the plasma via an ESI Apex IR desolvating nebulizer. Analyses were made in static mode, simultaneously measuring $^{26}$Mg, $^{25}$Mg, and

$^{24}$Mg isotopes. Measurements were performed in medium mass resolution mode in order to avoid the $CN^+$ interference on $^{26}$Mg. A 500 ppb solution typically gave a $^{24}$Mg signal of 14 V; the blank contribution to this signal was typically <0.01 V of $^{24}$Mg. Instrumental mass bias and drift are accounted for by following a standard-sample bracketing procedure. Sample solutions were diluted to ± 10% of the standard concentrations. Samples were bracketed using the Dead Sea magnesium (DSM-3) standard (Galy et al., 2003). Each sample was measured 3–6 times. Isotope ratios are expressed in δ notation as per mil (‰) deviation from DSM-3.

$$\delta^{26}\mathrm{Mg} = \left[\frac{\left(^{26}\mathrm{Mg}/^{24}\mathrm{Mg}\right)_{\mathrm{sample}}}{\left(^{26}\mathrm{Mg}/^{24}\mathrm{Mg}\right)_{\mathrm{standard}}} - 1\right] \times 1000$$

The external precision of the Mg analyses was determined by repeated measurements of the Cambridge-1 standard over 5 different days of analytical measurements (n = 46; $\delta^{26}$Mg = −2.60 ± 0.08‰ and $\delta^{25}$Mg = −1.34 ± 0.05‰ (2σ)). This value is within error of the accepted $\delta^{26}$Mg value for Cambridge-1 [−2.58 ± 0.14‰ (Galy et al., 2003)]. The accuracy was verified by analyses of basalt standards (USGS) processed through the same dissolution and purification procedure as the samples (see Table 1). Multiple measurements on all samples have comparable precision that is better than 0.12‰ (2σ).

## 4. Results

The $\delta^{26}$Mg values of all samples are between −1.59 and −2.09‰ (average of −1.76 ± 0.13‰, 1σ, n = 12) except for subsample Pl–Q of Sample A, which has a heavier $\delta^{26}$Mg value of −0.82‰ (Table 1, Fig. 2). These samples are all isotopically light relative to recent estimates for the Earth's mantle [−0.25 ± 0.07‰ (Teng et al., 2010a)] and the upper continental crust [−0.22‰ (Li et al., 2010)]. In Sample A, the $\delta^{26}$Mg values of subsamples from zones Px, Phl, and Px–Q–Pl are very similar, ranging from −1.69 to −2.09‰. Subsample Pl–Q is the furthest from the magma–carbonate contact and has the heaviest $\delta^{26}$Mg value of −0.82‰, ~1‰ heavier than the rest of the xenoliths. Three subsamples from Sample B, which represents a Px–Q–Pl lithology, yield $\delta^{26}$Mg values between −1.59 and −1.68‰. This is similar to the Mg isotopic composition in zones Px, Phl and Px–Q–Pl in Sample A (Fig. 3). Those samples with the lightest $\delta^{26}$Mg value have the highest pyroxene (and hence Mg) content. The $\delta^{25}$Mg vs. $\delta^{26}$Mg cross plot is illustrated in Fig. 4.

**Table 1**
Mg isotopic composition of the xenolith samples collected from the Fish Springs cinder cone, Sierra Nevada. All errors (2σ) are 2 standard deviations of the mean; n is the number of measurements for each sample, (r) is a replicate analysis.

| Specimen | Sample | MgO (wt.%) | $\delta^{26}$Mg | 2SD | $\delta^{25}$Mg | 2SD | n |
|---|---|---|---|---|---|---|---|
| A (zoned) | Px-1 | 13.5 | −1.72 | 0.05 | −0.91 | 0.04 | 3 |
| | Px-2 | 13.5 | −1.69 | 0.03 | −0.86 | 0.06 | 3 |
| | Px-2 (r) | 13.5 | −1.81 | 0.04 | −0.94 | 0.03 | 3 |
| | Px-3 | 14.5 | −1.82 | 0.02 | −0.94 | 0.03 | 3 |
| | Phl-1 | 20.0 | −1.88 | 0.06 | −0.98 | 0.01 | 3 |
| | Phl-1 (r) | 20.0 | −1.73 | 0.02 | −0.92 | 0.03 | 3 |
| | Phl-2 | 16.0 | −2.09 | 0.05 | −1.08 | 0.00 | 3 |
| | Px-Q-Pl-rich | 8.5 | −1.85 | 0.02 | −0.98 | 0.03 | 3 |
| | Px-Q-Pl-poor | 0.9 | −0.82 | 0.10 | −0.42 | 0.05 | 6 |
| B (unzoned) | B-1 | 3.4 | −1.60 | 0.06 | −0.83 | 0.08 | 3 |
| | B-1 (r) | 3.4 | −1.68 | 0.12 | −0.86 | 0.08 | 3 |
| | B-2 | 4.3 | −1.59 | 0.09 | −0.82 | 0.03 | 3 |
| | B-3 | 3.4 | −1.65 | 0.03 | −0.86 | 0.03 | 3 |

| Standard | $\delta^{26}$Mg | 2SD | $\delta^{25}$Mg | 2SD | n |
|---|---|---|---|---|---|
| Cambridge-1 | −2.60 | 0.08 | −1.34 | 0.05 | 46 |
| BIR | −0.30 | 0.04 | −0.16 | 0.03 | 3 |
| BCR | −0.45 | 0.06 | −0.23 | 0.06 | 3 |
| BHVO | −0.26 | 0.05 | −0.14 | 0.04 | 3 |

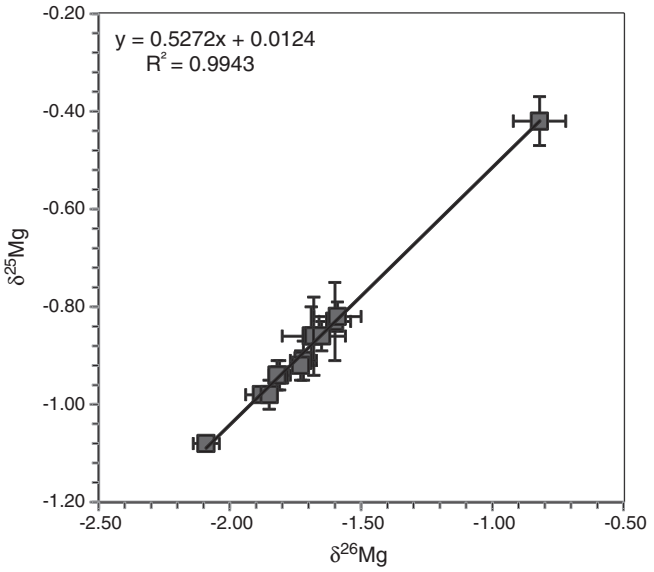


**Fig. 4.** $\delta^{26}$Mg vs. $\delta^{25}$Mg plot for the xenolith samples.

## 5. Discussion

The two most important results are as follows. First, all samples are depleted in $^{26}$Mg relative to average values for the upper continental crust (Tipper et al., 2008; Li et al., 2010) and published values for granitoid rocks (e.g., Shen et al., 2009; Li et al., 2010). Second, in Sample A the heaviest $\delta^{26}$Mg value is observed in the zone (Pl–Q) farthest from the carbonate wallrock. In order to explain these results we consider the following three scenarios.

### 5.1. Large equilibrium isotope fractionation

The first possibility is that the isotopically light Mg is the result of equilibrium isotopic fractionation between the minerals and a fluid/magma with normal, mantle-like isotopic signatures. This would require a fractionation factor Δ of −1.7‰, where $\Delta = \delta^{26}\mathrm{Mg}_{\mathrm{endoskarn}} - \delta^{26}\mathrm{Mg}_{\mathrm{fluid}}$. Ti-in-quartz thermometry on the Pl–Q and Px–Q–Pl zones yields temperatures between 510 and 570 °C (Dyer et al., 2011), which are lower than the temperature for water-saturated granite formation. These temperatures are thus minimum bounds on the original magmatic temperatures at which endoskarn formation occurred and may be too high for equilibrium isotope fractionation of Mg between phases (Liu et al., 2010). For example, no significant fractionation (<0.1‰) was observed between minerals during differentiation of granitic magmas (Liu et al., 2010) or at subsolidus conditions involving eclogites and peridotites (Li et al., 2011). Limited isotopic differences are observed between most mafic silicate mineral pairs, such as clinopyroxene, olivine, and orthopyroxene (Handler et al., 2009; Yang et al., 2009; Young et al., 2009; Liu et al., 2011). Significant high temperature fractionations have been observed between mineral pairs, such as spinel–olivine (Δ ~ 0.25–0.8‰), omphacite–garnet (1.14‰), and phengite–garnet (1.25–1.47‰) (Young et al., 2009; Li et al., 2011; Liu et al., 2011; Wang et al., 2012). However, the similar isotopic compositions of pyroxene-rich and phlogopite-rich zones in Sample A indicate that the isotopic variations are not related to phlogopite–pyroxene fractionations, and given that phlogopite forms by hydrous metasomatism of pyroxene, the similar isotopic signatures further suggest that no significant fractionations occurred between the fluid and the mafic minerals.

### 5.2. Kinetic equilibrium fractionation

A second scenario is the role of kinetic isotope fractionation (disequilibrium), wherein gradients in chemical potential or temperature drive diffusive re-equilibration in the solid or liquid states (Richter et al., 2008; Lundstrom, 2009; Richter et al., 2009a,b; Huang et al., 2010). In general, because the light isotope has a higher mean velocity than a heavier isotope at a given temperature (kinetic energy), isotopic zonation is expected to develop whenever a chemical or thermal gradient is imposed, even if the gradient is at a steady state. Thermally-driven diffusion is called "Soret"-type if it occurs in a liquid or "thermal migration" if it occurs in a multiphase system (Richter et al., 2009b). In Soret-type or thermal migration diffusion experiments, the heavy isotope concentrates in the cold granitic magma end while the light isotope remains in the hot basaltic end, suggesting preferential diffusion of isotopically heavy Mg from the hot, Mg-rich end to the cold, Mg-poor end (Richter et al., 2008). However, these predictions do not reproduce our observations. In Sample A, the pyroxenite (Px) zone represents the cold end (closest to wallrock), but it is isotopically light relative to the plagioclase–quartz (Pl–Q) zone which represents the hot end (magma). In any case, the temperature gradient across our sampling transect of <10 cm in Sample A was probably negligible because the thermal diffusion lengthscale during skarn formation is much greater (>100 m). Thermal migration effects are thus unlikely to have been significant on the lengthscales of our sampling.

Our observations also do not match those expected for Mg diffusion driven by a chemical gradient. In this scenario, the higher effective diffusivities of the light isotope would result in larger diffusive lengthscales for the light isotope compared to the heavy isotope. Therefore, Mg isotopes would be expected to become progressively lighter "downstream" of the Mg gradient (i.e., towards the granodioritic pluton), as has been seen in Li and Mg isotopes (Teng et al., 2006; Richter et al., 2008). In the case of Sample A, Mg isotopes are relatively constant before becoming heavier toward the magma body (Pl–Q zone), where the pyroxene-mode and hence Mg concentration are lowest. This is opposite to the expected behavior of Mg if it is controlled by chemical diffusion. We note that this discussion does not rule out the permeable flow of fluids (which follows D'Arcy's law and hence would mathematically have the form of diffusion) as the mechanism of introducing Mg into the granodiorite; it only rules out differential isotopic diffusion *through* fluids or solids as being responsible for the observed Mg isotope fractionations.

### 5.3. Source control

A third scenario is that the Mg isotopic systematics is determined by the interaction between granodioritic magma and dolomitic wallrock with distinct Mg isotopic compositions. Based on petrographic and geochemical studies, Dyer et al. suggested that these skarns and endoskarns formed by granodioritic magma reacting with dolomitic wallrock. Indeed, the $\delta^{26}$Mg values of carbonates are significantly lighter than those of the mantle and most igneous rocks (Galy et al., 2002; Buhl et al., 2007; Higgins and Schrag, 2010; Immenhauser et al., 2010; Teng et al., 2010a). For example, most limestones have $\delta^{26}$Mg values between −2.5 and −4.5‰ and dolomites between −1 and −2.5‰ (Galy et al., 2002; Buhl et al., 2007; Immenhauser et al., 2010). The $\delta^{26}$Mg values of all pyroxene-rich and phlogopite lithologies (−1.60 and −2.09‰) fall in the range of dolomite (Galy et al., 2002; Buhl et al., 2007; Higgins and Schrag, 2010), which we interpret as independent evidence for reaction with dolomitic wallrock. In particular, the constancy of the $\delta^{26}$Mg value in the pyroxene-rich and phlogopite lithologies suggests that the Mg in these lithologies is dominantly derived from the dolomitic wallrock (Fig. 5). The intermediate $\delta^{26}$Mg value in the Pl–Q zone of −0.8‰ suggests that the pyroxene might have been partially derived by replacement of primary plutonic biotite or hornblende, thus explaining the mixed Mg isotopic signature of the Pl–Q zone.

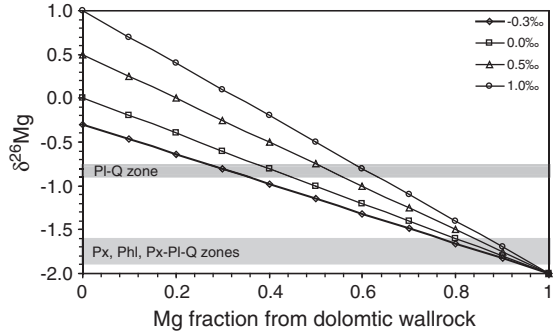


**Fig. 5.** Mixing model showing relative contribution of Mg from isotopically light dolomitic wallrock and isotopically heavy endmembers. Granitic endmember having mantle-like values is shown in bold. Heavier isotopic endmembers, representing magmas with larger pelitic components, are also shown for completeness.

The relative contribution of Mg from dolomitic wallrock and granodioritic magma can be estimated using a simple mixing model. Assuming that the $\delta^{26}$Mg values of the granodioritic magma and dolomitic wallrock are −0.3‰ and −2‰, respectively, mass balance suggests that approximately 70% of the Mg in the Pl–Q zone derives from the magma, whereas >90% of the Mg in the Px, Phl and Px–Pl–Q zones derive from the carbonate host rock (Fig. 5). For completeness, we also consider mixing with pelitic endmembers in Fig. 5, but mixing with pelitic endmembers would not generate a pyroxene-bearing lithology so it is not worth considering any further.

These results suggest that the Mg isotopic systematics in the endoskarns is best explained by mixing between isotopically heavy Mg in the magma and isotopically light Mg in the carbonate wallrock. Correlations between Mg isotopes and radiogenic isotopes in granitic differentiation series in plutonic rocks were interpreted to reflect mechanical mixing between endmembers rather than kinetic isotope effects (Shen et al., 2009). In the case of endoskarns, Mg is introduced into the pluton by the porous flow of fluids derived from the decarbonating country rock, rather than by bulk assimilation of the country rock.

## 6. Conclusions

We investigated Mg isotope systematics in endoskarn xenolith samples from the Pleistocene Fish Springs cinder cone in the Sierra Nevada. The endoskarns are composed of four mineralogic zones (from the contact into the interior): a pyroxenite zone at the wallrock–magma contact, a phlogopite zone, a plagioclase–quartz–pyroxene zone, and a plagioclase–quartz zone. All zones have Mg isotopic compositions lighter than peridotitic mantle. In detail, the Mg isotopic compositions of the pyroxene-rich and phlogopite-bearing zones are uniformly light. However, the Mg isotopic composition increases in the plagioclase–quartz zone, which is furthest from the contact and contains only sparse amounts of pyroxene. These isotopic anomalies are most easily explained by source effects rather than kinetic or equilibrium isotope fractionations. We suggest that the light Mg isotopes represent mixing of Mg between a granodioritic magma and dolomitic wallrock, the latter characterized by light Mg isotopes. Such mixing occurs through the fluid transport of Mg from the country rock into the magma, and not by bulk assimilation of the country rock.

## Acknowledgments

This research was supported by an NSF grant to Lee (EAR-0918577). Q.Z.Y. acknowledges UC Davis Start-up funds and NASA Planetary Major

Equipment grants as a supplement to NNX08AG57G, which enabled the acquisitions of the instruments used in this study.

## References


Allard, P., et al., 1991. Eruptive and diffuse emissions of $CO_2$ from Mount Etna. Nature 351 (6325), 387–391.

Bateman, P.C., 1961. Granitic formations in the east-central Sierra Nevada near Bishop. California Geological Society of America Bulletin, 72, pp. 1521–1537.

Beard, B.L., Glazner, A.F., 1995. Trace element and Sr and Nd isotopic composition of mantle xenoliths from the Big Pine Volcanic Field, California. J. Geophys. Res. 100 (B3), 4169–4179.

Berner, R.A., 2003. The long-term carbon cycle, fossil fuels and atmospheric composition. Nature 426, 323–326.

Blondes, M.S., Reiners, P.W., Ducea, M.N., Singer, B.S., Chesley, J., 2008. Temporal-compositional trends over short and long time-scales in basalts of the Big Pine Volcanic Field, California. Earth Planet. Sci. Lett. 269 (1–2), 140–154.

Brenot, A., Cloquet, C., Vigier, N., Carignan, J., France-Lanord, C., 2008. Magnesium isotope systematics of the lithologically varied Moselle river basin, France. Geochim. Cosmochim. Acta 72 (20), 5070–5089.

Buhl, D., Immenhauser, A., Smeulders, G., Kabiri, L., Richter, D.K., 2007. Time series $\delta^{26}$Mg analysis in speleothem calcite: kinetic versus equilibrium fractionation, comparison with other proxies and implications for palaeoclimate research. Chem. Geol. 244 (3–4), 715–729.

Chadwick, J.P., et al., 2007. Carbonate assimilation at Merapi Volcano, Java, Indonesia: insights from crystal isotope stratigraphy. J. Petrol. 48 (9), 1793–1812.

Dasgupta, R., Hirschmann, M.M., 2010. The deep carbon cycle and melting in Earth's interior. Earth Planet. Sci. Lett. (Frontiers) 298, 1–13.

Ducea, M., 2001. The California Arc: thick granitic batholiths, eclogitic residues, lithospheric-scale thrusting, and magmatic flare-ups. GSA Today 11, 4–10.

Dyer, B., Lee, C.-T.A., Leeman, W.P., Tice, M., 2011. Open-system behavior during pluton–wall-rock interaction as constrained from a study of endoskarns in the Sierra Nevada Batholith, California. J. Petrol. 52 (10), 1987–2008.

Fulignati, P., Marianelli, P., Santacroce, R., Sbrana, A., 2000. The skarn shell of the 1944 Vesuvius magma chamber. Genesis and P–T–X conditions from melt and fluid inclusion data. Eur. J. Mineral. 12 (5), 1025–1039.

Galy, A., Bar-Matthews, M., Halicz, L., O'Nions, R.K., 2002. Mg isotopic composition of carbonate: insight from speleothem formation. Earth Planet. Sci. Lett. 201 (1), 105–115.

Galy, A., et al., 2003. Magnesium isotope heterogeneity of the isotopic standard SRM980 and new reference materials for magnesium-isotope-ratio measurements. J. Anal. At. Spectrom. 18, 1352–1356.

Handler, M.R., Baker, J.A., Schiller, M., Bennett, V.C., Yaxley, G.M., 2009. Magnesium stable isotope composition of Earth's upper mantle. Earth Planet. Sci. Lett. 282 (1–4), 306–313.

Higgins, J.A., Schrag, D.P., 2010. Constraining magnesium cycling in marine sediments using magnesium isotopes. Geochim. Cosmochim. Acta 74 (17), 5039–5053.

Huang, F., et al., 2010. Isotope fractionation in silicate melts by thermal diffusion. Nature 464 (7287), 396–400.

Huang, K.-J., Teng, F.-Z., Wei, G.-J., Ma, J.-L., Bao, Z.-Y., 2012. Adsorption- and desorption-controlled magnesium isotope fractionation during extreme weathering of basalt in Hainan Island, China. Earth Planet. Sci. Lett. 359–360, 73–83.

Immenhauser, A., et al., 2010. Magnesium-isotope fractionation during low-Mg calcite precipitation in a limestone cave — field study and experiments. Geochim. Cosmochim. Acta 74, 4346–4364.

Kerrick, D.M., 2001. Present and past nonanthropogenic $CO_2$ degassing from the solid earth. Rev. Geophys. 39 (4), 565–585.

Kistler, R.W., Bateman, P.C., Brannock, W.W., 1965. Isotopic ages of minerals from granitic rocks of the central Sierra Nevada and Inyo Mountains. California Geological Society of America Bulletin, 76, pp. 155–164.

Lee, C.T.A., Morton, D.M., Kistler, R.W., Baird, A.K., 2007. Petrology and tectonics of Phanerozoic continent formation: from island arcs to accretion and continental arc magmatism. Earth Planet. Sci. Lett. 263 (3–4), 370–387.

Lee, C.-T.A., et al., 2013. Continental arc–island arc fluctuations, growth of crustal carbonates, and long-term climate change. Geosphere 9 (1), 21–36.

Li, W.-Y., et al., 2010. Heterogeneous magnesium isotopic composition of the upper continental crust. Geochim. Cosmochim. Acta 74, 6867–6884.

Li, W.-Y., Teng, F.-Z., Xiao, Y., Huang, J., 2011. High-temperature inter-mineral magnesium isotope fractionation in eclogite from the Dabie orogen, China. Earth Planet. Sci. Lett. 304, 224–230.

Liao, K., Morton, D.M., Lee, C.-T.A., 2012. Geochemical diagnostics of metasedimentary dark enclaves: a case study from the Peninsular Ranges Batholith, California. Int. Geol. Rev. http://dx.doi.org/10.1080/00206814.2012.753684.

Ling, M.-X., et al., 2011. Homogeneous magnesium isotopic composition of seawater. Rapid Commun. Mass Spectrom. 25, 2828–2836.

Liu, S.-A., Teng, F.-Z., He, Y., Ke, S., Li, S., 2010. Investigation of magnesium isotope fractionation during granite differentiation: implication for Mg isotopic composition of the continental crust. Earth Planet. Sci. Lett. 297 (3–4), 646–654.

Liu, S.-A., Teng, F.-Z., Yang, W., Wu, F.-Y., 2011. High-temperature inter-mineral magnesium isotope fractionation in mantle xenoliths from the North China craton. Earth Planet. Sci. Lett. 308 (1–2), 131–140.

Lundstrom, C., 2009. Hypothesis for the origin of convergent margin granitoids and Earth's continental crust by thermal migration zone refining. Geochim. Cosmochim. Acta 73 (19), 5709–5729.

Martel, S.J., Harrison, T.M., Gillespie, A.R., 1987. Late Quaternary vertical displacement rate across the Fish Springs fault, Owens Valley fault zone, California. Quat. Res. 27 (2), 113–129.

Mordick, B., Glazner, A., 2006. Clinopyroxene thermobarometry of basalts from the Coso and Big Pine volcanic fields, California. Contrib. Mineral. Petrol. 152 (1), 111–124.

Pogge von Strandmann, P.A.E., 2008. Precise magnesium isotope measurements in core top planktic and benthic foraminifera. Geochem. Geophys. Geosyst. 9. http://dx.doi.org/10.1029/2008GC002209.

Pogge von Strandmann, P.A.E., et al., 2008. The influence of weathering processes on riverine magnesium isotopes in a basaltic terrain. Earth Planet. Sci. Lett. 276 (1–2), 187–197.

Richter, F.M., Watson, E.B., Mendybaev, R.A., Teng, F.Z., Janney, P.E., 2008. Magnesium isotope fractionation in silicate melts by chemical and thermal diffusion. Geochim. Cosmochim. Acta 72 (1), 206–220.

Richter, F.M., Dauphas, N., Teng, F.-Z., 2009a. Non-traditional fractionation of non-traditional isotopes: evaporation, chemical diffusion and Soret diffusion. Chem. Geol. 258 (1–2), 92–103.

Richter, F.M., et al., 2009b. Isotopic fractionation of the major elements of molten basalt by chemical and thermal diffusion. Geochim. Cosmochim. Acta 73 (14), 4250–4263.

Shen, B., Jacobsen, B., Lee, C.-T.A., Yin, Q.-Z., Morton, D.M., 2009. The Mg isotopic systematics of granitoids in continental arcs and implications for the role of chemical weathering in crust formation. Proc. Natl. Acad. Sci. 106 (49), 20652–20657.

Teng, F.-Z., McDonough, W.F., Rudnick, R.L., Walker, R.J., 2006. Diffusion-driven extreme lithium isotopic fractionation in country rocks of the Tin Mountain pegmatite. Earth Planet. Sci. Lett. 243 (3–4), 701–710.

Teng, F.-Z., et al., 2010a. Magnesium isotopic composition of the Earth and chondrites. Geochim. Cosmochim. Acta 74 (14), 4150–4166.

Teng, F.-Z., Li, W.-Y., Rudnick, R.L., Gardner, L.R., 2010b. Contrasting lithium and magnesium isotope fractionation during continental weathering. Earth Planet. Sci. Lett. 300 (1–2), 63–71.

Tipper, E.T., Galy, A., Bickle, M.J., 2006a. Riverine evidence for a fractionated reservoir of Ca and Mg on the continents: implications for the oceanic Ca cycle. Earth Planet. Sci. Lett. 247 (3–4), 267–279.

Tipper, E.T., et al., 2006b. The magnesium isotope budget of the modern ocean: constraints from riverine magnesium isotope ratios. Earth Planet. Sci. Lett. 250, 241–253.

Tipper, E.T., Galy, A., Bickle, M.J., 2008. Calcium and magnesium isotope systematics in rivers draining the Himalaya-Tibetan-Plateau region: lithological or fractionation control? Geochim. Cosmochim. Acta 72 (4), 1057–1075.

Wang, S.-J., Teng, F.-Z., Williams, H.M., Li, S.-G., 2012. Magnesium isotopic variations in cratonic eclogites: origins and implications. Earth Planet. Sci. Lett. 359–360, 219–226.

Wimpenny, J., et al., 2010. The behaviour of Li and Mg isotopes during primary phase dissolution and secondary mineral formation in basalt. Geochim. Cosmochim. Acta 74 (18), 5259–5279.

Yang, W., Teng, F.-Z., Zhang, H.-F., 2009. Chondritic magnesium isotopic composition of the terrestrial mantle: a case study of peridotite xenoliths from the North China craton. Earth Planet. Sci. Lett. 288 (3–4), 475–482.

Young, E.D., Tonui, E., Manning, C.E., Schauble, E., Macris, C.A., 2009. Spinel–olivine magnesium isotope thermometry in the mantle and implications for the Mg isotopic composition of Earth. Earth Planet. Sci. Lett. 288 (3–4), 524–533.